Inhibitory Copper Binding Site on the Spinach Cytochrome b_6f Complex: Implications for Q_o Site Catalysis†

Sudha Rao B. K.‡ Alexei M. Tyryshkin,§ Arthur G. Roberts,‡ Michael K. Bowman,§ and David M. Kramer*,‡

Institute of Biological Chemistry, Washington State University, 289 Clark Hall, Pullman, Washington 99164-6340, and Macromolecular Structure & Dynamics, WR Wiley Environmental Molecular Sciences Laboratory, Pacific Northwest National Laboratories, Richland, Washington 99352-0999

Received August 23, 1999; Revised Manuscript Received November 18, 1999

ABSTRACT: The isolated cytochrome (cyt) b_6f complex from spinach is inhibited by Cu^{2+} with a K_D of about 1 μM at pH 7.6 in the presence of 1.6 μM decyl−plastoquinol (C_{10}−PQH_2) as a substrate. Inhibition was competitive with respect to C_{10}−PQH_2 but noncompetitive with respect to horse heart cyt *c* or plastocyanin (PC). Inhibition was also pH-sensitive, with an apparent p*K* at about 7, above which inhibition was stronger, suggesting that binding occurred at or near a protonatable amino acid residue. Equilibrium binding titrations revealed ca. 1.4 tight Cu^{2+} binding sites with a K_D of about 0.5 μM and multiple (>8) weak (K_D > 50 μM) binding sites per complex. Pulsed electron paramagnetic resonance (EPR) techniques were used to identify probable binding sites for inhibitory Cu^{2+}. A distinct enhancement of the relaxation time constant for the EPR signal from bound Cu^{2+} was observed when the cyt *f* was paramagnetic. The magnitude and temperature-dependence of this relaxation enhancement were consistent with a dipole interaction between Cu^{2+} and the cyt *f* (Fe^{3+}) heme at a distance of between 30 and 54 Å, depending upon the relative orientations of Cu^{2+} and cyt *f* heme g-tensors. Two-pulse electron spin−echo envelope modulation (ESEEM) and 4-pulse 2-dimensional hyperfine sublevel correlation (2D HYSCORE) measurements of Cu^{2+} bound to isolated cyt b_6f complex indicated the presence of a weakly coupled nitrogen nucleus. The nuclear quadrupole interaction (NQI) and the hyperfine interaction (HFI) parameters identified one Cu^{2+} ligand as an imidazole nitrogen of a His residue, and electron−nuclear double resonance (ENDOR) confirmed the presence of a directly coordinated nitrogen. A model of the 3-dimensional structure of the cytochrome b_6f complex was constructed on the basis of sequences and structural similarities with the mitochondrial cyt bc_1 complex, for which X-ray structures have been solved. This model indicated three possible His residues as ligands to inhibitory Cu^{2+}. Two of these are located on the "Rieske" iron−sulfur protein protein (ISP) while the third is found on the cyt *f* protein. None of these potential ligands appear to interact directly with the quinol oxidase (Q_o) binding pocket. A model is thus proposed wherein Cu^{2+} interferes with the interaction of the ISP protein with the Q_o site, preventing the binding and subsequent oxidation of plastoquinonol. Implications for the involvement of ISP "domain movement" in Q_o site catalysis are discussed.

The cytochrome[1] (cyt) *bc* complexes constitute a major part of the energy transduction machinery in many living cells (for reviews, see refs *1*−*3*). They catalyze the transfer of electrons from reduced quinone (ubihydroquinone or ubiquinol in mitochondria, plastoquinol in chloroplasts, and menaquinol in many bacteria) to a soluble protein (cyt *c*, plastocyanin, or, in some cases, a high-potential iron−sulfur protein, or HIPIP). This transfer is tightly coupled to the pumping of protons across the membrane that contains the complex, and the resulting electrochemical potential of protons drives the synthesis of ATP via a chemiosmotic circuit. The cyt *bc* complexes are broken into two classes: bc_1 and b_6f types (for reviews see refs *1*−*3*), although forms intermediate between the bc_1 and b_6f complexes have been found in some bacteria (*4*−*7*). The most intensively studied

† This work was supported by a Herman Frasch Foundation Award and by the U.S. Department of Energy (DE-FG03-98ER20299) to D.M.K. Pacific Northwest National Laboratory (PNNL) is a multiprogram national laboratory operated by Battelle Memorial Institute for the U.S. Department of Energy under Contract DE-AC06-76RLO 1830. This research was supported by Associated Western Universities, Inc., Northwest Division (AUW NW) under Grant DE-FG06-89ER-75522 or DE-FG06-92RL-12451 with the U.S. Department of Energy and by the Office of Biological and Environmental Research, U.S. Department of Energy. The W. R. Wiley Environmental Molecular Sciences Laboratory (EMSL) is a national scientific user facility sponsored by the U.S. DOE's Office of Biological and Environmental Research and located at PNNL.

* To whom correspondence should be addressed. Tel.: ++(509) 335-4964. Fax: ++(509) 335-7643. E-mail: dkramer@wsu.edu.

‡ Washington State University.

§ Pacific Northwest National Laboratories.

[1] Abbreviations: C_{10}−PQH_2, decyl−plastoquinol-10; cw, continuous wave; cyt, cytochrome; DMSO, dimethyl sulfoxide; EDTA, ethylenediaminetetraacetic acid; EPR, electron paramagnetic resonance; ENDOR, electron−nuclear double resonance spectroscopy; ESEEM, electron spin−echo envelope modulation spectroscopy; Fe_2S_2, the two iron−two sulfur redox center of the Rieske iron sulfur protein; HEPES, *N*-[2-hydroxyethyl]piperazine-*N*′-[2-ethanesulfonic acid]; HFI, hyperfine interaction; HYSCORE, 4-pulse 2-dimensional hyperfine sublevel correlation EPR spectroscopy; ISP, the "Rieske" iron−sulfur protein; NQI, nuclear quadrupole interaction; PQ, plastoquinone; PQH_2, plastoquinol; Q_i, the quinone reductase site of the cyt b_6f and cyt bc_1 complexes; Q_o, the quinol oxidase site of the cyt b_6f and cyt bc_1 complexes; UQ, ubiquinone; UQH_2, ubiquinol.

10.1021/bi991974a CCC: $19.00
Published on Web 03/03/2000

version of these complexes is the bc_1 complex, which is found in mitochondria and proteobacteria. The cyt b_6f complex is found in chloroplasts and cyanobacteria. Both bc_1 and b_6f complexes contain four redox-active, metal centers: one heme *c*, one Rieske-type Fe_2S_2 center, and low- and high-potential *b*-type hemes, termed cyt b_L and cyt b_H, respectively. These metal centers are found in three proteins: heme *c* in cyt c_1 (or cyt *f* in b_6f); the Fe_2S_2 center in the Rieske iron−sulfur protein (ISP); the *b* hemes in a single cyt *b* (or cyt b_6 in b_6f) protein. In the cyt b_6f complex, as well as the *bc* complexes from some bacteria (e.g. heliobacteria), the cyt *b* protein is split into a heme binding protein and subunit IV. Many bacteria contain this minimal, three- or four-protein structure. The bc_1 complexes from mitochondria contain additional proteins that serve poorly understood structural or regulatory functions. The sequences within each family of complexes are highly conserved with the exception of the *c*-type cyts which have little similarity in sequence or 3-dimensional structure (see refs *8*−*10*). In fact, the *bc*-type complex from *Heliobacillus mobilis* is reported to possess a diheme *c*-type cyt (*7*) although the basic mechanism for the complex appears to be conserved (*6*).

The working model for most research on *bc* complexes is the Q-cycle, first proposed by Mitchell and later modified by several groups (see reviews in refs *2*, *3*, and *11*−*16*). In the Q-cycle, two protons are pumped across the energetic membrane for each electron transferred from hydroquinone to a high-potential acceptor (i.e. cyt *c* in mitochondria, plastocyanin, or cyt c_6 in chloroplasts). The electron transfer is a bifurcated process, as reviewed recently by Brandt (*17*). One electron from the quinol bound at site Q_o is transferred to the Fe_2S_2 center, while the other is forced to flow through the low-potential cyt *b* chain to reduce a quinone in site Q_i. Both protons from site Q_o are ultimately released on the *p*-side of the membrane while quinone reduction at the Q_i site picks up protons from the *n*-side of the membrane. Thus, because the bifurcation of the electron flow at the Q_o site allows only one electron from quinol to pass to the high-potential electron acceptor, it doubles the expected number of protons pumped per electron and accounts for the high efficiency of energy transduction by the *bc* complexes.

The recent publication of high-resolution X-ray structures of mitochondrial cyt bc_1 complexes has greatly accelerated progress in understanding the function of these enzymes (*18*−*22*). One notable feature of the crystal structures is a variation in the position of the "head" (or hydrophilic extension) of the ISP. Depending on the crystal form and the presence of inhibitors, the ISP can adopt a conformation that places the Fe_2S_2 cluster essentially in contact with the Q_o site in cyt *b*, termed the $ISP_{cyt\ b}$ conformation, or in contact with its other redox partner (i.e. cyt c_1 in the case of the cyt bc_1 complex), termed the $ISP_{cyt\ c}$ conformation (*17*, *19*, *23*). The presence of two distinct ISP conformations led to the "domain movement" hypothesis where the ISP pivots back and forth to "gate" electron transfer, forcing the two electrons on the quinol to be transferred through different pathways (*17*, *19*, *23*). In the $ISP_{cyt\ b}$ conformation, quinol is bound at the Q_o site and transfers one electron to the oxidized Fe_2S_2 center. Subsequent transfer of this electron is prevented because the ISP in this conformation is distant (∼31 Å) from cyt c_1. Thus, the Q_o site semiquinone remains at the site long enough to reduce cyt b_L, which in turn reduces cyt b_H and finally a quinone or semiquinone bound at the Q_i site. Only upon full oxidation of Q_o site quinol does the ISP pivot and make close contact with cyt c_1, allowing electron transfer to mobile cyt *c*.

Such motion has been confirmed in fluorescence-quenching experiments (*24*) and by EPR measurements on partially oriented samples of the *bc* complexes (*52*, *53*). Two conformations of the ISP, broadly consistent with those found in X-ray diffraction structures, have been found in the cyt b_6f complex from chloroplasts (*25*) and in bacterial cyt *bc* complexes from *Chlorobium* and *Bacillus* species (*26*). The presumption is strong that these two conformations are the active states in the functional model derived from the X-ray structures. However, that remains to be settled. They conceivably could be an "active" and a "denatured" conformation of the ISP. Because cyt c_1 and *f* have no structural homology aside from the heme binding motif, cyt *f* and Q_o could be close enough that the ISP need not pivot. On the other hand, the pivoting would be expected in all cyt *bc* complexes if it were an essential requirement for the bifurcated electron flow. Thus, the question of whether the ISP pivots in all *bc*-type complexes is important for understanding the general mechanism of energy transduction. The cyt b_6f complex is an especially good model system for comparative studies because its differences with the bc_1 complexes have been well-studied—in particular, the X-ray structures of cyt *f* and ISP from the cyt b_6f complex have recently been solved (*9*, *27*, *28*).

In addition, mechanisms have been proposed for the cyt b_6f complex that differ significantly, and in some cases radically, from those proposed for the cyt bc_1 complexes (e.g. refs *3*, *29*, and *30*−*35*), and testing whether prevalent mechanistic models based on the cyt bc_1 complex are also applicable to the cyt b_6f complex will go a long way toward resolving such issues. One of the most prevalent hypothesis is that the cyt b_6f complex is a facultative proton pump, i.e., that electron transfer through the complex is coupled to proton pumping at low light intensities, where ATP is needed, but not at high light intensities, where presumably less ATP is needed light (see refs *36*−*43*). Such a "bypass switch" would radically alter the energy budget of the plant as well as our understanding of the mechanism of the cyt b_6f complex (see discussion in ref *44*). We have shown that, regardless of the in vivo energy status of the plant, electron transfer through the cyt b_6f complex appears tightly coupled to the pumping of protons (*45*, *46*; Sacksteder, C. A., and Kramer, D. M., manuscript in preparation). We thus maintain a working model for the cyt b_6f complex that is similar to that proposed for its mitochondrial analogue.

Inhibitors of cyt bc_1 and b_6f complexes have been useful tools in the elucidation of the mechanism of these complexes (*2*, *47*, *48*). Most of these inhibitors are structural analogues of quinones and block the Q_o or Q_i sites (*49*, *50*). The continuing utility of these inhibitors was illustrated by the recent X-ray crystal structures of the mitochondrial bc_1 complex (*18*, *19*, *51*), where stigmatellin and antimycin A were used to identify the quinone/quinol binding pockets. In addition, the effects of a number of Q_o site inhibitors on the conformation of the ISP have provided support for the domain movement hypothesis (*19*, *25*, *26*).

Certain metal ions, including aluminum, cadmium, copper, lead, mercury, silver, and zinc, constitute a distinct class of

inhibitors of the cyt bc_1 and b_6f complexes (*52*, *53*), but relatively little is known about the structural basis of their action. The most extensive studies to date were performed by Link and von Jagow (*53*) on the effects of Zn^{2+} on the bovine mitochondrial cyt bc_1 complex. These authors found that inhibition by Zn^{2+} was pH-dependent, suggesting that this metal binds near an amino acid residue with a p*K* of about 7. They also argued that the Zn^{2+} binding site was unlikely to be on the ISP since tight binding remained in ISP-depleted complexes. Inhibition by Zn^{2+} was found to be noncompetitive with respect to both cyt *c* and quinol, meaning that increasing the concentrations of these substrates did not overcome inhibition by the metal. These data led the authors to suggest that Zn^{2+} binds at a site distinct from those of other inhibitors, possibly blocking a channel required to allow protons produced from ubiquinol (UQH_2) oxidation to escape to the aqueous phase.

In this paper we show Cu^{2+} inhibits the spinach cyt b_6f complex, competing with substrate quinol, by binding to a His residue, most likely on the cyt *f* protein or the ISP, but not at the Q_o site itself. We conclude that Cu^{2+} is likely an inhibitor of ISP domain movements and discuss implications of these findings for the function of the cyt b_6f complex. A preliminary report on some this research was presented at the XIth International Congress on Photosynthesis (*54*).

MATERIALS AND METHODS

Thylakoid Preparation. Spinach thylakoids were prepared by a method modified from ref *55*. Spinach leaves were either purchased from a local market or grown in a green house under 900 μmol of photons·m^{-2}·s^{-1}, 12 h of daylight, watered daily, and fertilized 3 times a week with Peters 15/30/15 solution. Similar results were obtained with both types of preparation. The spinach leaves were rinsed with distilled, deionized water and then ground in a medium containing 50 mM *N*-[2-hydroxyethyl]piperazine-*N*′-[2-ethanesulfonic acid] (HEPES), pH 7.6, 5 mM $MgCl_2$, 300 mM sorbitol, and 10 mM NaCl. The resulting suspension was strained through 8 layers of cheesecloth, and the filtrate was poured into 200 mL centrifuge bottles and centrifuged for 15 min at 5000 rpm in a Sorval SLA1500 rotor. The pellet was suspended in suspension buffer containing 50 mM HEPES, pH 7.6, 330 mM sorbitol, 10 mM KCl, and 5 mM $MgCl_2$ to a concentration of 3 mg chlorophyll·mL^{-1}. The resulting thylakoid membranes were either used immediately or were suspended in suspension buffer with 10% dimethyl sulfoxide (DMSO) as a cryoprotectant and stored at −80 °C for future use. The chlorophyll content of the thylakoids was determined as described in ref *56*.

Isolation of Cyt b_6f Complex. Cytochrome b_6f complex was isolated from spinach thylakoids essentially by the procedure described by Hurt and Hauska (*57*). Following the sucrose density gradient, purified cyt b_6f complex was collected and concentrated to 50 μM cyt *f* using a Centricon concentrator, molecular weight cutoff of 10 000 Da, and then stored at −80 °C in 50 mM HEPES−NaOH, pH 7.6 containing 30 mM octyl glucoside. The choice of HEPES buffer was critical since many other buffers chelate Cu^{2+}, preventing strong interaction with the complex (*58*). The concentration of the cyt b_6f complex was determined by measuring the reduced (20 mM ascorbate) minus oxidized (250 μM ferricyanide) absorbance difference spectrum, using an extinction coefficient of 25 mM^{-1} cm^{-1} for the α-band at 554 nm (*59*).

Cytochrome b_6f Activity. Activities of the isolated cyt b_6f complex under various conditions were determined from the rates of reduction of horse heart cyt *c* or spinach plastocyanin (PC) by plastoquinol-10 (C_{10}−PQH_2) at room temperature, as described in ref *57*. A 2 mL volume of a 10 mM solution of decyl−plastoquinone (C_{10}−PQ, Sigma) in 1:1 ethanol/ethylene glycol was reduced by addition of 2 mg of sodium borohydride. After 10 min of incubation on ice, the solutions were acidified by addition of 5 μL of concentrated HCl, to remove excess reductant (*60*). The kinetics of C_{10}−PQH_2 oxidation were measured spectrophotometrically, using a Cary 17 spectrophotometer (modified for computer control), by observing absorbance changes at 285 nm, using extinction coefficients for the plastoquinol and plastoquinone species of 14 and 4 mM^{-1} cm^{-1} respectively (*61*). The kinetics of horse heart cyt *c* reduction were similarly measured by observing the absorbance change at 551 nm, using an extinction coefficient of 17 mM^{-1} cm^{-1} (*62*). Reactions were initiated by addition of C_{10}−PQH_2 using a plastic spatula, resulting in the loss of no more than 4 s of the initial absorbance changes. Initial slopes of the kinetic curves were taken between 5 and 15 s after the addition of C_{10}−PQH_2. Kinetics obtained under each assay condition, but in the absence of cyt b_6f complex, were subtracted from corresponding traces containing enzyme to account for nonenzymatic (or background) electron-transfer rates. Such corrections were especially important in the presence of added copper, which accelerated nonenzymatic electron transfer.

Equilibrium Binding Titrations. The strengths and stoichiometries of Cu^{2+} binding to the isolated spinach cyt b_6f complex were estimated by equilibrium binding titrations. Frozen stocks of cyt b_6f complex were thawed and diluted to 1 μM cyt *f* with buffer containing 50 mM HEPES, pH 7.6, 15 mM n-octyl glucoside, and 0.24 mM sodium ferricyanide (to maintain both the complex and added copper in their oxidized states), and 1 mL aliquots were transferred to microcentrifuge tubes. Small aliquots of a $CuCl_2$ solution were slowly added to the samples with constant, gentle stirring on ice. After incubation on ice in total darkness for approximately 30 min, the samples were ultracentrifuged at 513 000*g* for 3 h in a Beckman Optima TLX ultracentrifuge. The bound copper pelleted with the protein, while free copper remained in the supernatant. The pellet and the supernatant fractions were treated separately with excess concentrated HCl and incubated overnight at 55 °C. The amounts of protein-bound and free Cu^{2+} were estimated with an atomic absorption spectrometer (model 2380, Perkin Elmer), calibrated using known copper standards.

Electron Paramagnetic Resonance. Continuous-wave and pulsed EPR experiments were performed with an X-band Bruker ESP-380e spectrometer equipped with a MD-5 dielectric resonator and an Oxford Instruments CF935 helium cryostat. A two-step phase cycle, $+(0,0)$, $-(\pi, 0)$, in the two-pulse sequence was used to eliminate interference from the electron free induction decay in the primary echo envelope. The length of a $\pi/2$ pulse was nominally 16 ns. A 2-dimensional electron spin−echo envelope modulation (ESEEM) experiment, 2-dimensional hyperfine sublevel correlation EPR spectroscopy (HYSCORE), with a sequence of four microwave pulses (*63*) was used to probe the envi-

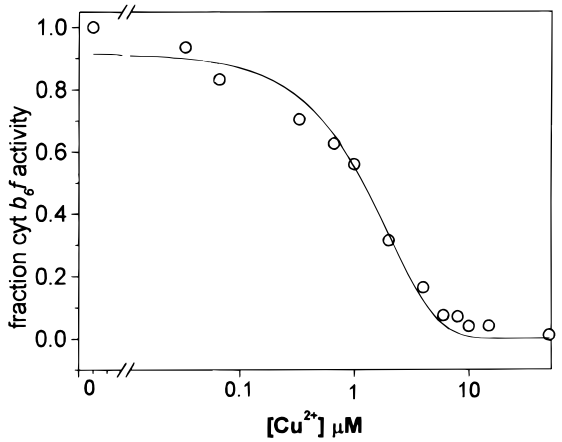

FIGURE 1: Inhibition of isolated b_6f complex by Cu^{2+} ions. Activity of isolated cyt b_6f complex was estimated as the initial rates of horse heart cyt *c* reduction measured at 551 nm upon addition of 0.33 μM $C_{10}-PQH_2$. The concentrations of cyt b_6f complex, cyt *c*, and $C_{10}-PQH_2$ were 15 nM, 25 μM, and 330 nM, respectively. Samples were suspended in 50 mM HEPES and 15 mM octyl glucoside, pH 7.6, as described in Materials and Methods.

ronment of the protein-bound Cu^{2+}. In addition to separating complex patterns of lines that overlap in the one-dimensional ESEEM spectra, the two-dimensional HYSCORE spectra are valuable for the assignment of ESEEM peaks to particular nuclei (*63*, *64*). A four-step phase cycling +(0,0,0,0), −(0,0,0 π), +(0,0,π, 0), and +(0,0,π, π) was used to remove unwanted echoes (*65*). Pulsed electron−nuclear double resonance (ENDOR) measurements were performed with the Davies sequence (*66*) using an ENI A-500 RF amplifier. Phase memory times (T_M) were measured using the 2-pulse sequence (*67*). Experimental data were processed using Bruker WIN-EPR software and the WinDS data processing program by Dr. A. V. Astashkin from the Institute of Chemical Kinetics and Combustion, Novosibirsk, Russia. EPR spectra were simulated with the Bruker SimFonia program to obtain *g* and *A* values of Cu^{2+}.

RESULTS

Inhibition of the Isolated cyt b_6f Complex by Cu^{2+}. Figure 1 shows that steady-state electron transfer from 0.33 μM $C_{10}-PQH_2$ to 25 μM horse heart cyt *c* was inhibited by Cu^{2+} with an apparent K_I of about 1 μM. Because Cu^{2+} is potentially reducible by the substrate ($C_{10}-PQH_2$), it could intercept electrons before they reach cyt *c*. To test for this possibility, the effect of Cu^{2+} on the reduction of cyt *c* was compared to its effect on $C_{10}-PQH_2$ oxidation. Figure 2 shows that, during the first 15 s after addition of $C_{10}-PQH_2$, the rate of cyt *c* reduction was proportional to that of $C_{10}-PQH_2$ oxidation, with a slope of approximately 1.8 mol of cyt *c* reduced/mol of $C_{10}-PQH_2$ oxidized. This relationship was reasonably maintained as [Cu^{2+}] was increased. On the minutes time scale, deviations of up to 20% developed between $C_{10}-PQH_2$ oxidation and cyt *c* reduction (data not shown) indicating that a fraction of $C_{10}-PQH_2$ electrons was diverted to other acceptors. The deviations were significantly (ca. 2-fold) smaller in the absence of O_2, suggesting that a fraction of electrons was shunted to O_2. Moreover, these data indicate that, at least at short assay times, the predominant effect of Cu^{2+} was to inhibit the cyt b_6f complex rather than act as an alternative electron acceptor.

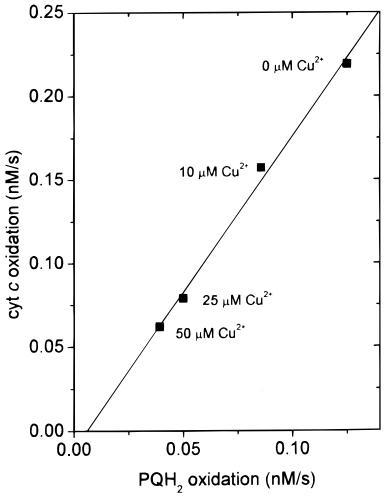

FIGURE 2: Comparison of the initial rates of cyt *c* reduction, monitored at 551 nm, with those of $C_{10}-PQH_2$ oxidation, monitored at 285 nm. The concentrations of cyt *c* and $C_{10}-PQH_2$ were kept constant at 25.8 and 1.6 μM, respectively, while the concentrations of added Cu^{2+} were increased from 0 to 50 μM. The concentration of Cu^{2+} used for each point is indicated next to each point. All assays were performed in 50 mM HEPES and 15 mM octyl glucoside, pH 7.6, in sealed cuvettes, deoxygenated with flowing Ar for 15 min before the start of each reaction. Other conditions were as described in Figure 1.

Figure 3A,B shows the effects on inhibition of varying the concentrations of cyt *c* and $C_{10}-PQH_2$. Cytochrome *c* produced a classical noncompetitive Lineweaver−Burk plot, indicating that the site of action of Cu^{2+} was distinct from the site of interaction of cyt *c* with the cyt b_6f complex (Figure 3A). Because similar K_I values were obtained from assays where either 1 or 10 μM PC was used as an acceptor (data not shown), we concluded that Cu^{2+} inhibition is also noncompetitive with respect to the physiological electron acceptor for the complex.

On the other hand, the Lineweaver−Burk plot in Figure 3B shows that $C_{10}-PQH_2$ competes with Cu^{2+}. These data indicate that the binding sites for Cu^{2+} and $C_{10}-PQH_2$ overlap or thermodynamically interact to disfavor simultaneous binding (see Discussion). In contrast, a strictly noncompetitive inhibition of the bc_1 complex by Zn^{2+} was observed by Link and von Jagow (*53*), indicating that increasing the concentrations of these substrates did not alter the strength of inhibition by the metal. In our experiments, the v_{max} for cyt *c* reduction in the absence of Cu^{2+} estimated from Figure 3B, using a relatively high concentration (21 μM) of cyt *c* and extrapolating to infinite [$C_{10}-PQH_2$], was about 16 s^{-1} and considering the pH-sensitivity of cyt b_6f activity (see below) was consistent with previous reports (e.g. ref *57*). The K_m for $C_{10}-PQH_2$ was approximately 330 nM in the absence of Cu^{2+} and increased to an apparent K_m about 2 μM in the presence of 10 μM Cu^{2+}. Replotting the slopes of the double-reciprocal plot versus the [Cu^{2+}], as described in e.g. Segel (*68*), yields an estimate of the true K_I for Cu^{2+} of 1−2 μM (not shown).

Dependence of Cu^{2+} Inhibition on pH. Figure 4 shows that the inhibition of isolated cyt b_6f complex by Cu^{2+} is pH-dependent, with an apparent p*K* of about 7, above which binding is pH-dependent. There may be a second p*K* at about pH 8, but instability of the enzyme prevented assays at higher pH values. Link and von Jagow (*53*) noted that inhibition

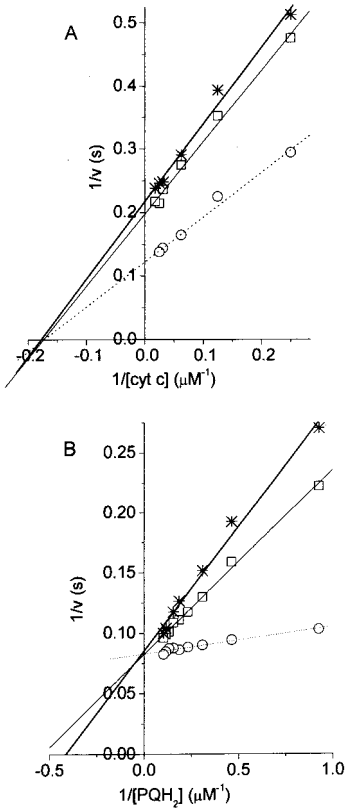

FIGURE 3: Analysis of the inhibition of the cyt b_6f complex by Cu^{2+}. (A) Lineweaver−Burk plot for inhibition of the cyt b_6f complex by Cu^{2+} as a function of cyt *c* concentration. Conditions were as above except that the concentration of $C_{10}-PQH_2$ was held at 1.6 μM, while the concentration of cyt c was varied between 4 and 56 μM. (B) Lineweaver−Burk plot for inhibition of the cyt b_6f complex by Cu^{2+} as a function of $C_{10}-PQH_2$ concentration. Samples contained 21 μM cyt *c* in 50 mM HEPES and 15 mM octyl glucoside, pH 7.8. The concentration of plastoquinol was varied between 1 and 10 μM. Kinetics were assayed at 0 (open circles), 10 (open squares), and 15 μM (asterisks) Cu^{2+}.

of cyt bc_1 complex by Zn^{2+} was also pH-dependent with a p*K* near 7, but in that case, K_I was pH-sensitive below 7. This indicates that the protonatable group controlling Cu^{2+} binding to the cyt b_6f complex becomes fully protonated below pH 7, whereas the group controlling the binding of Zn^{2+} to the cyt bc_1 complex becomes fully deprotonated above pH 7. Because the p*K* values for protonatable groups can be dramatically affected by their local environments, it is not possible to assign a particular type of amino acid as the cause of the observed pH dependence. Nevertheless, it is reasonable to consider His, Cys, and Tyr residues. Figure 4 also shows the pH dependence of cyt b_6f activity, which is similar to that previously observed for the isolated cyt b_6f complex (e.g. ref *69*) or the cyt bc_1 complex (e.g. ref *53* and references within). As has been discussed previously (e.g. refs *69* and *70*−*72*), the rate of quinol oxidation in cyt b_6f and bc_1 complexes is likely controlled at low pH by the deprotonation of the quinol or by the pH dependence of the redox poise of the Q_o site quinol:semiquinone couple. At high pH, the rate of quinol oxidation becomes pH-independent, most likely because of deprotonation of an amino acid residue involved in catalysis (see also discussions in refs *70*, *72*, and *73*). Unlike the case of Zn^{2+} inhibition of the cyt bc_1 complex, the protonatable group controlling

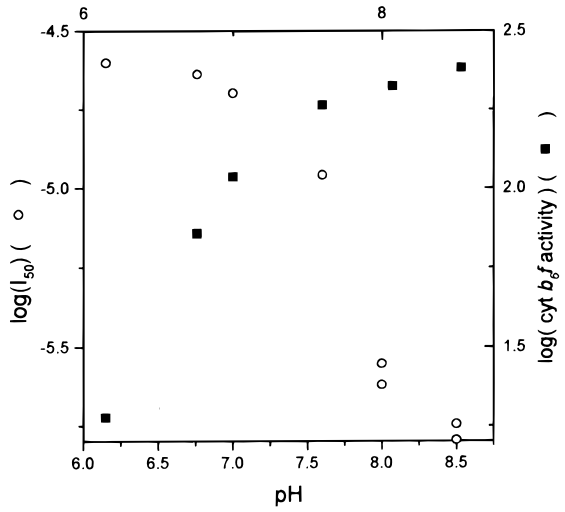

FIGURE 4: pH dependencies of cyt b_6f activity and Cu^{2+} inhibition. The open circles represent the I_{50} of Cu^{2+} effect obtained from b_6f enzyme kinetics; $[C_{10}-PQH_2] = 1.68$ μM, and [cyt *c*] = 21.8 μM in buffer solutions of respective pH. The solid squares show the pH dependence of cyt b_6f complex activity (expressed as μM cyt *c* reduced/μM $C_{10}-PQH_2$/nM b_6f/h). The samples were prepared with 1.5 μM $C_{10}-PQH_2$, 20 μM cyt *c*, and 10 nM cyt b_6f complex, in 50 mM HEPES and 15 mM octyl glucoside, at different pH values.

Cu^{2+} binding is clearly distinct from that governing cyt b_6f activity.

Reversibility of Cu^{2+} Inhibition. It is well-known that Cu^{2+}, when reduced to Cu^{+} by endogenous reductants, can catalyze the production of activated oxygen species that can irreversibly damage enzymes (for a review of such effects in photosynthetic systems, see ref *74*). The observation of Link and von Jagow (*53*) that Cu^{2+} inhibition of the mitochondrial cyt bc_1 complex was only partially reversible by addition of EDTA may be related to these effects. To test for such oxidative damage in the cyt b_6f complex, we assessed the reversibility of Cu^{2+} inhibition. At 4 °C, under atmospheric oxygen, addition of 20 μM Cu^{2+} to isolated cyt b_6f essentially completely inhibited the $C_{10}-PQH_2$ to cyt *c* electron transfer. Incubation of inhibited samples for 30 min in the presence of 800 μM EDTA resulted in about 90% recovery of activity with respect to similarly treated control samples (data not shown). We conclude that the major effects of Cu^{2+} are due to direct, reversible binding to the complex but that long-term exposure to Cu^{2+} in the presence of oxygen may irreversibly damage the complex.

Equilibrium Binding of Cu^{2+} to Isolated Cyt b_6f Complex. Equilibrium binding assays were performed to determine the number and affinity of Cu^{2+} binding sites on the cyt b_6f complex. Figure 5 shows a Scatchard plot of binding data. A best-fit Scatchard curve indicates the presence of approximately 1.4 high-affinity Cu^{2+} sites per complex with a K_D in the range of 0.5 μM and numerous (>8) low-affinity Cu^{2+} binding sites with $K_D > 50$ μM. Within the noise level, these data are consistent with the existence of one high-affinity site with a K_D similar to the K_I for Cu^{2+} inhibition of the complex (see above), while the low-affinity sites are likely due to nonspecific binding of Cu^{2+} to the protein, lipids, or detergent.

EPR Relaxation Properties of Bound Cu^{2+}. Pulsed EPR was used to probe the location of bound Cu^{2+} with respect to other cyt b_6f complex redox groups. To avoid interference

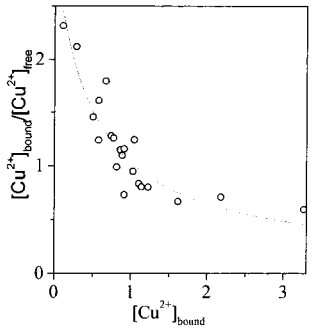

FIGURE 5: Scatchard plot for binding of Cu^{2+} to the isolated cyt b_6f complex. The concentration of cyt b_6f complex was 1 μM in 50 mM HEPES, pH 7.6. Other experimental details are as in the Materials and Methods. Reasonable fits to the Scatchard plot were obtained with two independent binding sites, one high-affinity (K_D = 0.5 μM) site binding about 1.4 Cu/complex, and >8 low-affinity (K_D > 50 μM) sites per cyt b_6f complex.

from relaxation of EPR signal associated with free Cu^{2+}, samples with measurable amounts of unbound Cu^{2+}, as detected by its distinct EPR spectrum, were discarded. Continuous-wave EPR assays (not shown) indicated that the bound Cu^{2+} was typical of a type II copper. A detailed report of its characteristics will be given elsewhere (Roberts, A., Bowman, M. K., and Kramer, D. M., submitted for publication). The cw EPR spectra spectra also showed that, as isolated, the cyt b_6f complex was in a partially reduced state; the cyt *f* heme was about 90% reduced (i.e. nonparamagnetic) while the ISP Fe_2S_2 center was approximately 50% reduced (i.e. paramagnetic) (see also ref *75*). This ratio of redox states is consistent with relative midpoint potentials for the two centers (*9*, *76*, *77*). Both cyt *f* and the Fe_2S_2 center were fully oxidized by addition of 100 μM sodium ferricyanide.

The temperature dependence of two-pulse echo decay times, T_M, taken at the maximum of the electron spin−echo detected EPR spectrum of Cu^{2+}, were found to be dependent on the redox state of the cyt b_6f complex (Figure 6). In fully oxidized samples, a pronounced minimum in T_M occurred near 8 K, consistent with an interaction of Cu^{2+} with fast-relaxing paramagnetic species (*67*, *78*−*80*). On the other hand, the semireduced samples showed little temperature dependence of T_M. Thus, the enhanced T_M of bound Cu^{2+} can be assigned to the interaction with the paramagnetic heme of cyt *f*.

The enhancement of T_M can be analyzed to provide estimates of spin−spin distance (*79*). The T_M of bound Cu^{2+} can be expressed in terms of contributions from cyt *f* and other sources, such that

$$\frac{1}{T_M} = \frac{1}{T_{M0}} + W_{dd}$$

where, T_{M0} is copper relaxation time in the absence of reduced cyt *f* and W_{dd} is the contribution due to paramagnetic cyt *f* heme. The W_{dd} term can be numerically simulated

$$W(\tau) = \exp\left(-\frac{\tau}{T_1}\right) * \left\langle\left(\left[\cosh(R\tau) + \frac{\sinh(R\tau)}{2RT_1}\right]^2 + \frac{D^2}{4R^2}\sinh^2(R\tau)\right)\right\rangle_\theta$$

on the basis of the following equation describing relaxation

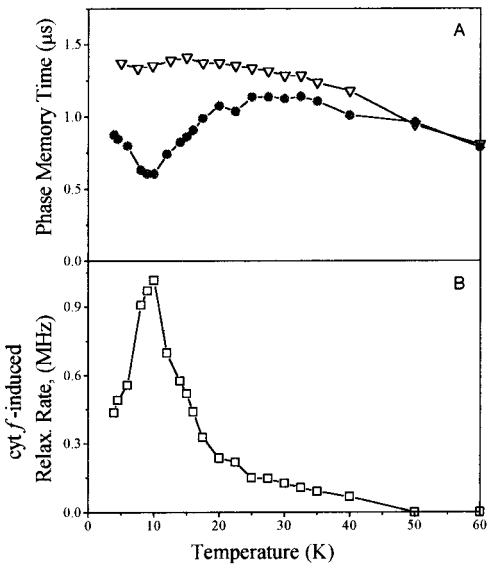

FIGURE 6: Dependence of copper phase memory relaxation times on temperature. (A) (closed circles) 100 μM Cu^{2+} with 100 μM cyt b_6f complex oxidized by 200 μM ferricyanide; (open triangles) 100 μM cyt b_6f complex as isolated with 100 μM Cu^{2+}. (B) The contribution of paramagnetic cyt *f* to the phase memory relaxation of copper measured as the difference in relaxation rates (reciprocals of the relaxation times) between the two curves in panel A. Relaxation times were measured from two-pulse electron spin−echo decays, microwave frequency of 9.71 GHz, at a magnetic field of 336.6 mT (the maximum of the copper spectrum). The two-pulse echo decays were fit by a smooth polynomial that was then subtracted from the data and used to normalize the data. The data were apodized to minimize the noise at long times and Fourier transformed, and a linear phase correction was applied. The Symphonia program was used to simulate the cw EPR spectra of Cu^{2+} to obtain *g* and *A* values.

enhancement in a 2-pulse echo, $W(\tau)$, due to electron−electron interaction between two spins (*79*):

$$D = \frac{\mu_0}{4\pi}\frac{g_1 g_2 \beta^2}{hr^3}(1 - 3\cos^2\theta)$$

Where

$$4R^2 = T_1^{-2} - D^2$$

and T_1 is the longitudinal relaxation time of cyt *f*. The term *D* is the dipole−dipole interaction between copper and the cyt *f* heme spins, *r* is the interspin distance, and θ is the angle between the direction of external magnetic field and a vector connecting the two species with *g*-factors g_1 and g_2. The expression is averaged over different orientations of the external magnetic field with respect to the complex for frozen solution samples. Theoretical analyses (*79*) show that $W(\tau)$ is a monotonic function and can be approximated over a wide range of τ values as an exponential:

$$W(\tau) \cong \exp(-W_{dd}\tau)$$

The value of W_{dd} can be calculated for a given interspin distance vector, *r*, and relaxation time T_1. This provides a means to estimate the distance *r* between the interacting species (*17*).

From the measurements in Figure 6, we would estimate the distance between the bound copper and cyt *f* heme to be

43 ± 2 Å if both species had isotropic *g*-factors equal to 2, if we observed all orientation of the pair relative to the magnetic field, and if T_1 of cyt *f* was orientation-independent. The real situation is more complicated. The *g*-factor of cyt *f* varies between 0.9 and 3.5 (ref *81* and references within) depending on orientation. In addition, the measurements were made at the maximum of the copper EPR spectrum, which roughly observes only those coppers whose $g_{||}$ axis is perpendicular to the applied magnetic field. We expect the Cu^{2+} to be oriented with respect to the cyt *f*, so only a selected set of orientations of the pair relative to the magnetic field contribute to the measurement. Furthermore, it is not known whether the T_1 of cyt *f* is isotropic, and we estimate that up to 10% of *cyt f* could have been in its oxidized state in the semireduced samples. These factors increase the uncertainties of the distance estimates but still allow us to set limits on the distance that will enable us to locate the site of Cu^{2+} binding in the cyt b_6f complex. The temperature range over which the cyt *f* affects the phase relaxation of the Cu^{2+} is fairly narrow and consistent with the T_1 being isotropic so we assume that it is in our analysis. We calculated the phase memory relaxation rates in the plane perpendicular to the unique *g*-value of the Cu^{2+} caused by dipolar interaction with cyt *f*. The distances required to produce the observed relaxation rates varied for different orientations of the Cu^{2+} and the heme of cyt *f* relative to each other. The minimum distance of 30 Å is found when the Cu^{2+} lies in the plane of the heme and the $g_{||}$ of Cu^{2+} pointed about 40° away from the heme. The largest distance of 54 Å occurs when the Cu^{2+} lies directly above the heme plane and the $g_{||}$ of Cu^{2+} is perpendicular to the Cu^{2+}−heme direction. These are broad but useful limits bounding the distance, *r*, between the Cu^{2+} and the heme of cyt *f* in the range 54 Å > *r* > 30 Å.

Characterization of Cu^{2+} Ligand Environments on Cyt b_6f Complex and Cyt f. Two-pulse ESEEM (*82*−*85*) is a well-established technique for the investigation of the local and ligand environments of protein-bound paramagnetic species. The spectra presented in Figure 7 were taken at 336.6 mT because this region was found to be relatively uncontaminated by contributions from species other than Cu^{2+}. Virtually identical spectra were obtained at several other field strengths (data not shown). The spectrum shows prominent low frequency peaks at 0.8, 1.58, and 4.15 MHz. The line 0.8 MHz is resolved into two, separate peaks at 0.67 and 0.9 MHz, in a 3-pulse stimulated echo spectrum (not shown). These lines are intense and narrow, a characteristic of a nitrogen with a predominantly isotropic hyperfine interaction that nearly cancels, and are typical of ^{14}N modulations observed from the remote (amido) N of an imidazole liganded to Cu^{2+} (*86*, *87*). No evidence was ever seen of combination bands that would indicate the presence of more than a single histidine ligand to the copper. The higher frequency peak at 14.35 MHz arises from weakly coupled protons, presumably from water or the protein. The low-frequency ESEEM lines exhibit an additive relationship, i.e., $0.67 + 0.9 \cong 1.58$ MHz. These lines are intense and narrow, a characteristic of a nitrogen whose isotropic hyperfine coupling nearly cancels the nuclear Zeeman interaction in one of the electron spin manifolds, i.e., $|a/2 \pm \nu_I| \cong 0$. Confirmation of the near cancellation condition comes also from the HYSCORE spectra (see below). In this case, the

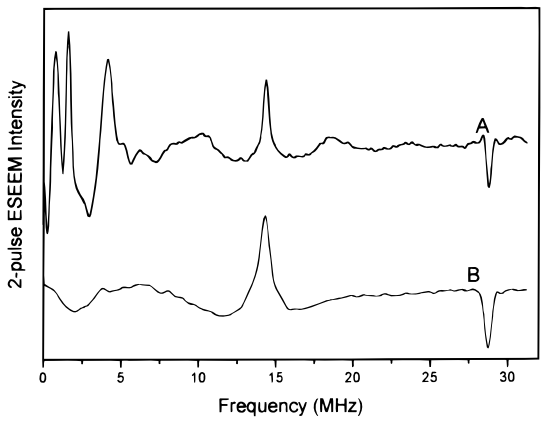

FIGURE 7: 2-pulse ESEEM spectra of bound and free copper: Trace A, 200 μM cyt b_6f complex, 375 μM ferricyanide, and 200 μM Cu^2; trace B, $CuCl_2$ in 50 mM HEPES buffer, pH 7.6. Cosine Fourier transforms of ESEEM were measured at 30 K with a microwave frequency of 9.70 GHz and magnetic field of 336.6 mT. The low-frequency region in trace A contains positive going peaks from a nitrogen as well as negative going peaks from difference combination lines of the nitrogen and of the protons. The peak near 28.7 MHz is the sum combination line from the protons. The two-pulse echo decays were fit by a smooth polynomial that was then subtracted from the data and used to normalize the data. The data were apodized to minimize the noise at long times and Fourier transformed, and a linear phase correction was applied. No deadtime reconstruction was performed, and each of the peaks has the expected inverted "feet" flanking it. These are most clearly evident around the proton peak at 14.25 MHz.

low frequencies correspond to the pure nuclear quadrupole (NQI) frequencies:

$$\nu_0 = 2k\eta \quad \nu_- = k(3 - \eta) \quad \nu_+ = k(3 + \eta)$$

Here 4*k* is the quadrupole coupling constant and η is the rhombicity parameter (*88*). Thus, $4k = 1.65$ MHz and $\eta = 0.81$ are the estimated values for the nitrogen interacting with the Cu^{2+} bound to cyt b_6f complex. For a predominantly isotropic hyperfine interaction close to the cancellation condition, the pure NQI frequencies in one electron spin manifold are usually accompanied in the opposite electron spin manifold by a double-quantum transition given by (*89*)

$$\nu_{dq} = 2\left[\left(\frac{a}{2} + \nu_I\right)^2 + k^2(3 + \eta^2)\right]^{1/2}$$

The intense line at 4.19 MHz is an obvious candidate for the ν_{dq} transition. Using the above estimation of quadrupole parameters, we estimate the isotropic hyperfine coupling of the nitrogen, $a = 1.81$ MHz. This value corresponds closely with the cancellation condition.

The spectrum of Cu^{2+} in HEPES buffer contains only proton peaks at the Zeeman frequency, $\nu_I = 14.3$ MHz due to weakly coupled protons (Figure 7, trace B). This indicates that the nitrogen modulations observed in the protein samples are from the protein not the buffer. This was confirmed by assays using protein samples prepared in 50 mM citrate buffer, pH 7.6, which resulted in spectra identical to those obtained in HEPES buffer (data not shown), confirming that the nitrogen peaks originate from the protein.

The HYSCORE spectra of Cu^{2+} bound to the cyt b_6f complex is shown in Figure 8. The intense ridge at 14.4 MHz

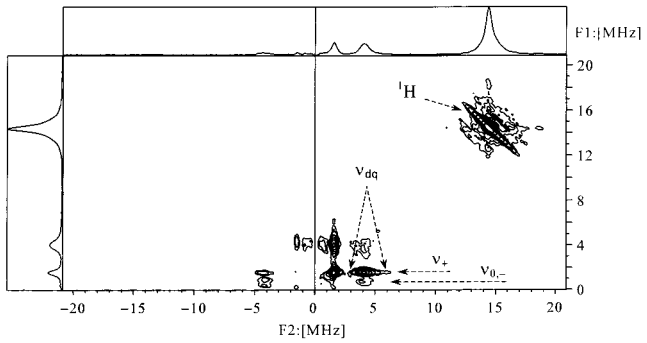

FIGURE 8: 2D HYSCORE spectra of copper bound to protein. The spectrum was taken with isolated cyt b_6f complex (200 μM), 375 μM ferricyanide, and 200 μM Cu^{2+} at 30 K with a microwave frequency of 9.71 GHz, magnetic field of 336.6 mT, and the interval between the first two pulses, τ, set at 104 ns.

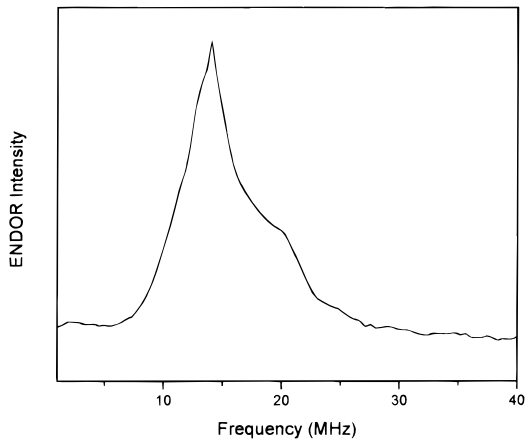

FIGURE 9: Pulsed ENDOR spectra of protein bound copper: 100 μM b_6f; pH 7.6; 100 μM copper. The maximum near 14.3 MHz is from weakly coupled protons while the high-frequency shoulder is from strongly coupled nitrogen. A relatively narrow initial pulse in the Davies ENDOR pulse sequence was used to attenuate the ENDOR response from weakly coupled protons. Experimental parameters were similar to those in Figure except that the inverting pulse to suppress proton frequencies was nominally 24 ns.

perpendicular to the diagonal is due to weakly coupled protons, and the low-frequency peaks are from nitrogen nuclei. Cross-correlation (nondiagonal) peaks are observed between the three low frequencies 0.67, 0.9, and 1.58 MHz and the higher frequency peak at 4.2 MHz. The three low frequencies arise from one of the electron spin manifolds, and the higher frequency (4.2 MHz) arises from the other. The cross-correlation peaks form ridges nearly parallel to the axes of the 2D-spectrum, which confirms that they are due to a nitrogen near the cancellation condition.

The quadrupole parameters estimated for the nitrogen ($4k = 1.65$ MHz, and $\eta = 0.81$) are characteristic of the remote amido nitrogen of an imidazole ring whose imino nitrogen is directly coordinated to Cu^{2+} (*90*). Thus, the ESEEM and HYSCORE measurements indicate that one of the ligands to Cu^{2+} in the cyt b_6f complex is the imidazole of a histidine residue. ESEEM spectroscopy at X-band can measure only the remote amido nitrogen of a liganded histidine, and thus, to confirm this assignment, we probed for the proximal imino nitrogen using pulsed ENDOR measurements (Figure 9). A symmetric proton peak at the proton Zeeman frequency of 14.3 MHz is partially suppressed using a single nonselective 24 ns preparation pulse as described in refs *91* and *92*. The high-frequency shoulder from 16.8 to 18.2 MHz is due to strongly interacting nitrogen(s).

No significant changes were observed between ENDOR measurements at different positions across the entire Cu^{2+} EPR spectrum. Thus, the directly coordinated nitrogen has a nearly isotropic hyperfine interaction of 35 MHz. The nitrogen coupling of this magnitude is typical of nitrogen directly coordinated to Cu^{2+} as expected for a histidine ligand.

DISCUSSION

It has been known for over four decades that trace metal ions can inhibit respiration, and Link and von Jagow (*53*) suggested that Zn^{2+} ions inhibit the electron transfer through the mitochondrial cyt bc_1 complex by blocking a proton channel from the Q_o site to the *p*-side aqueous phase. In addition, metal ions, particularly Cu^{2+} have been shown to inhibit photosynthesis at the level of electron transfer. In recent papers, the primary site of copper action on higher plant photosynthesis has been ascribed to PS II (*93*−*98*), but PS I (*99*), the cyt b_6f complex (*100*), and ferredoxin (*95*), have also been implicated as sites of action. More recently, bacterial reaction centers were shown to bind Zn^{2+} (*101*) and Cd^{2+} (*102*), modulating electron transfer by restricting protein (*101*) and proton (*102*) movements. In this paper, Cu^{2+} was shown to inhibit electron transfer through the isolated spinach cyt b_6f complex. At low C_{10}−PQH_2 concentrations, inhibition occurred at micromolar concentrations of Cu^{2+} (Figures 1 and 3). Inhibition was essentially reversible by addition of EDTA (data not shown), indicating that the primary effects of Cu^{2+} were caused by direct interaction rather than by the production of reactive oxygen species. We note that the effects of Cu^{2+} on isolated complexes is likely to differ from that on intact thylakoids, where diffusion of Cu^{2+} across the thylakoid membrane may be restricted; other components may chelate added Cu^{2+}, or other factors may sensitize the complex to Cu^{2+} inhibition.

Comparison of Zn^{2+} Effects on Cyt bc_1 and Cu^{2+} Effects on Cyt b_6f Complexes. We have found that inhibition of the cyt b_6f complex by Cu^{2+} differs significantly from Zn^{2+} inhibition of the cyt bc_1 in a number of respects. Inhibition of the b_6f complex by Cu^{2+} appeared competitive with the reductant, C_{10}−PQH_2 (Figure 3A), but not with the oxidants, PC (not shown) or cyt *c* (Figure 3B), whereas Zn^{2+} inhibition of cyt bc_1 was noncompetitive with either reductant or oxidant; i.e., the affinity of Zn^{2+} for the cyt bc_1 complex was unaffected by varying the concentrations of these substrates (*53*). The pH dependence of Zn^{2+} inhibition of cyt bc_1 roughly followed the pH dependence of quinol oxidase activity (*53*), whereas inhibition of the cyt b_6f complex by Cu^{2+} was pH dependent only above p*K* 7 (Figure 4). Thus, our data suggest that the respective metal binding sites are distinct.

Proposed Structural Basis for Inhibition of Cyt b_6f Complex by Cu^{2+}. One large advantage of the present experimental system is that Cu^{2+} is paramagnetic, allowing the use of sophisticated EPR techniques to probe its binding environment. The dependence of the EPR relaxation properties (the phase memory relaxation times) of bound Cu^{2+} on temperature and the redox state of the complex place bound

Cu^{2+} near the cyt *f* heme, with a center−center distance between 30 and 54 Å (Figure 6). Dipole−dipole distance measurements between bound Cu^{2+} and the Fe_2S_2 cluster were not possible because the Fe_2S_2 center longitudinal relaxation time was found to be unfavorable (data not shown), and similar measurements between cyt *b* and bound Cu^{2+} are presently being attempted. Nevertheless, the distance estimates so far gained allow us to make several conclusions about the nature of Cu^{2+} interaction with the complex.

To determine which His residues could ligate inhibitory Cu^{2+} and result in the observed dipole−dipole interaction with the cyt *f* heme, we modeled the cyt b_6f complex protein structure and location of redox components on the basis of the structural homology to the cyt bc_1 complexes. The primary sequences of cyt *b* and subunit IV were aligned using CLUSTAL (*103*). The structure of the spinach cyt b_6f complex ISP was modeled to the high-resolution X-ray structure for the cyt bc_1 complex presented in ref *19* with the program DALI (*104*−*107*). The corresponding amino acids were superimposed onto the cyt bc_1 structure. Because there is scant homology between cyt *f* and cyt c_1 (*108*), we assumed that the cyt *f* heme is in the same relative position as cyt c_1 but that the plane of the cyt *f* heme was oriented 30° to the membrane, as measured in refs *109* and *110*. Also considered in our model was the likely PC binding site, which was placed so that it was free from obstruction from other subunits. Ubbnik et al. (*111*) and Fernandez-Velasco et al. (*112*) have shown that PC likely binds to the cyt *f* protein in close contact with the heme edge, and bound PC does not come into close proximity to H142. This is consistent with our results that Cu^{2+} inhibition is noncompetitive with respect to cyt *c* or PC. It is expected that the ISP also interacts with the cyt *f* protein near the heme at a site distinct from the PC docking site (*112*). The cyt bc_1 crystal structures (*19*, *113*, *114*) show that the cyt c_1 membrane spanning region occurs at the periphery of the dimer, whereas the Q_o sites are located near the monomer−monomer interface. Considering that the 8 Å resolution projection map of the cyt b_6f complex shows a general shape similar to that of the cyt bc_1 complex (*115*), it is reasonable to suggest that the cyt *f* membrane span is also located on the periphery of the dimer and thus distant from the Q_o site.

Overall, our model is similar to that presented in ref *116*, and essentially the same conclusions are drawn from each. Figure 10 is a cartoon of the resulting model structure, showing estimated locations of all 13 His residues on cyt *b*, subunit IV, cyt *f*, and the Fe_2S_2 protein. Spinach residue numbering, preceded by subunit designation, is used throughout the following. The range of possible cyt *f* heme−Cu^{2+} distances estimated by the phase memory relaxation time encompasses much of the cyt *f* protein, the ISP, and parts of cyt *b* protein and subunit IV. Fortunately, the majority of these residues can be eliminated as Cu^{2+} ligands. ISP-H10, cyt *b*-H29, and subunit IV-H24 are expected to be near the stromal side of the membrane and thus too distant for the observed dipole−dipole interaction with the cyt *f* heme. Cyt *f*-H24 is an axial ligand to the heme and thus far too near to explain the EPR data. In addition, modification or distortion of the heme axial ligand by Cu^{2+} binding would cause noticeable alterations in the cyt *f* absorbance and EPR spectra,

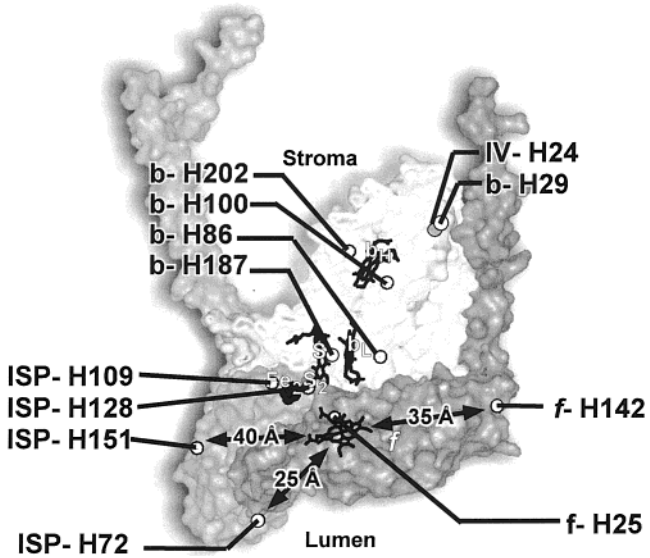

FIGURE 10: Model of spinach cyt b_6f complex derived from its sequence and structural homology with the cyt bc_1 complex as described in the text. The distances were measured from the Fe of cyt *f* to the respective backbone Cα of the His residues, denoted by the open circles. Residues are numbered according to the spinach sequence, preceded by designation of their respective subunit: ISP = iron sulfur protein; IV = subunit IV; f = cyt *f*. Prosthetic and other species are denoted as the following: b_H = high potential cyt *b* heme; b_L = low potential cyt *b* heme; *f* = cyt *f* heme; Fe_2S_2 = "Rieske" iron sulfur cluster cluster; S = stigmatellin.

whereas no such changes were observed upon addition of up to 10 μM Cu^{2+} (unpublished results). ISP-H109 and ISP-H128 on the ISP are ligands to the Fe_2S_2 cluster. On the basis of previous EPR experiments using a range of Q_o site inhibitors (e.g. refs *117*−*119*), we expect large effects on the EPR spectrum of the cluster, particularly the g_z feature. Since no such changes were observed (*120*), we conclude that Cu^{2+} does not bind to the Fe_2S_2 ligands. Likewise, cyt *b*-H86, cyt *b*-H187, cyt *b*-H100, and cyt *b*-H202 are ligands to cyt b_L and b_H, respectively, are unlikely Cu^{2+} ligands since no changes in *b*-type cyt EPR (*120* and unpublished results) or visible absorbance spectra (unpublished data) were observed upon Cu^{2+} binding. This leaves H142 on the cyt *f* protein and H72 and H151 of the ISP as potential Cu^{2+} ligands. These potential assignments are relatively robust in the modeling procedure, since all but the most dramatic structural changes (e.g. the removal or addition of a transmembrane spanning helix) yield essentially the same conclusions.

The structure of the water-soluble portion of turnip cyt *f* (*9*) shows that the H142 is found at the surface of the cyt *f* protein, near the (truncated) hydrophobic tail at a center−center distance from the heme of 35 Å, consistent with the EPR-estimated distances. Comparison of primary sequences of cyt *f* proteins from various species shows that the region around H142 is well conserved, although we hasten to add that the entire cyt *f* protein is well conserved. In addition, substitutions of the residue corresponding to H142 occur in several species, most notably changes to Ser and Tyr in *Chlamydomonas reinhardtii* and *Pisum sativum*, respectively. Interestingly, Zn^{2+} was found to bind to the *Phormidium laminosum* cyt *f* crystal structure at the amino acid equivalent to H142 (H150) (*10*), but no Zn^{2+} binding was found in the *C. reinhardtii* cyt f crystal despite the fact that the crystal

was grown in elevated [Zn^{2+}] (PDB file 1CFM; E. Berry, personal communication). We note that preliminary studies in our laboratory have shown that the *P. sativum* cyt b_6f complex was approximately 10-fold less sensitive to Cu^{2+} inhibition (unpublished data). Although a more detailed investigation, including assays at varying $C_{10}-PQH_2$ concentrations, will be necessary to make any firm conclusions, these results are consistent with a role for this region of the protein in Cu^{2+} binding.

Our sequence and structural alignments indicate that residues H151 and H72 of the cyt b_6f complex ISP are likely to be analogous to S148 and D80 of the cyt bc_1 ISP. In the high-resolution structures of the mitochondrial cyt bc_1 complex (*18*, *19*, *113*), both of these residues are surface exposed and face into the aqueous phase on the *p*-side of the membrane (i.e. analogous to the thylakoid lumen). Neither of these residues appears to interact with other subunits of the complex, although it is conceivable that a Cu^{2+} bound to D80 could also have a ligand from the cyt c_1 protein. On the other hand, considering the lack of homology between cyt *f* and cyt c_1, we cannot exclude the possibility that H72 and H151 play an important role in the interaction of the ISP with cyt *f*.

Implications for the Function of the Cyt b_6f Complex. The overall conclusion we reach from the structural studies described above is that, despite the observed competition between inhibitory Cu^{2+} and substrate quinol, Cu^{2+} appears to bind quite distant from the Q_o site. As discussed in depth in Segel (*68*), the binding sites for a competitive inhibitor does not necessarily overlap the binding site for its competitive substrate but may instead affect activity via allosteric modulation. Briefly, binding of an inhibitor to a distinct inhibition site can cause a conformational change that alters the binding affinity for substrate at the catalytic site. In this case, by thermodynamic principle, binding of substrate to the active site will decrease the binding affinity of the inhibitor to its binding site, leading to a competitive relationship. We argue that such behavior might be expected within the context of recent "domain movement" models for Q_o site catalysis. Because of the high homology between the cyt bc_1 and b_6f complexes complex, it is likely that the quinol oxidation at the cyt b_6f Q_o site proceeds by a similar mechanism. Indeed, there is strong evidence from oriented EPR experiments on isolated cyt b_6f complex that the orientation of the ISP is affected by the occupancy of the Q_o site (*25*). For discussion, we will use the terms $ISP_{cyt\ b}$ and $ISP_{cyt\ f}$ for the ISP conformations analogous to the $ISP_{cyt\ b}$ and $ISP_{cyt\ c}$ in the cyt bc_1 complex.

Two points concerning the cyt bc_1 complex structures are especially relevant to interpretation of our data. First, the binding of substrates to the Q_o site affects the conformation of the ISP, with the $ISP_{cyt\ b}$ conformation being adopted when substrate quinol is bound. It thus follows that the ISP conformational change will have a significant contribution to the thermodynamics of substrate binding, and thus, the binding affinity of substrate should depend on the propensity of the ISP to adopt the $ISP_{cyt\ b}$ conformation. Second, the adoption of the $ISP_{cyt\ c}$ (or $ISP_{cyt\ f}$) position involves interactions with the cyt c_1 (cyt *f*) proteins. Thus, any changes in the conformation of cyt *c* (cyt *f*) could affect substrate quinol binding by altering the propensity of ISP to adopt its various conformational changes. Indeed, arguments have been made that cyt *f* also adopts multiple conformations (ref *116* and references within).

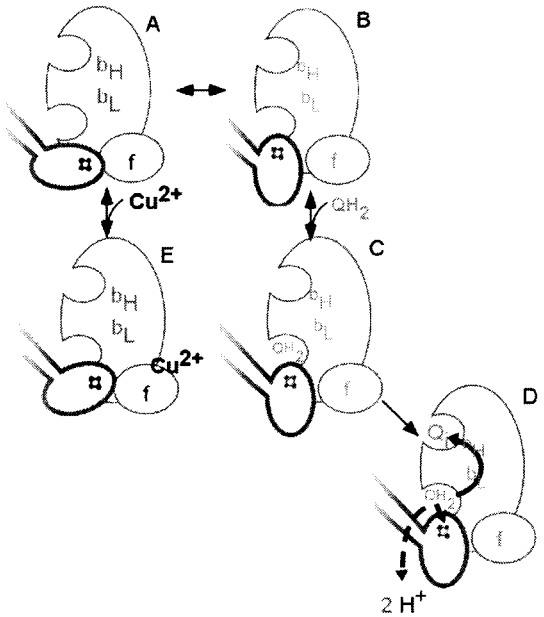

FIGURE 11: Model for inhibition of quinol oxidation at the cyt b_6f complex by Cu^{2+}. In the absence of substrate and inhibitor, the ISP will pivot between at least two conformations (A and D). Changes in ISP conformation will also affect the conformation of the other subunits it interacts with, namely cyt *b* and cyt *f*. In the A conformation, Cu^{2+} can bind, possibly to cyt *f*, forming the E conformation which has low affinity for substrate quinol. In the D conformation, substrate quinol can bind, forming state C, which can catalyze quinol oxidation leading to state D. This model allows Cu^{2+} to bind at a site distant from the Q_o site while acting competitively with quinol.

We thus propose the model illustrated in Figure 11, where copper binds either to H142 on cyt *f* or to the H72 or H151 of the ISP, favoring a conformation of the $ISP_{cyt\ f}$ that disfavors quinol binding. In effect, this will destabilize the $ISP_{cyt\ b}$ conformation and lower the affinity of the Q_o site for $C_{10}-PQH_2$. On the other hand, binding of $C_{10}-PQH_2$ to the Q_o site will favor the formation of the $ISP_{cyt\ b}$ and ultimately lower the affinity of the complex for Cu^{2+}, making Cu^{2+} competitive with $C_{10}-PQH_2$. Along these same lines, Utschig et al. (*101*) have suggested that Zn^{2+} binding hinders electron transfer in bacterial reaction center by interfering with protein domain movements. A reasonable test of our model, which is currently being made in our laboratories, would be to assay Cu^{2+}-induced changes in the orientations of the cyt *f* and ISP redox groups or, complementarily, if conformational changes in these subunits affect the binding properties of Cu^{2+} to the complex.

ACKNOWLEDGMENT

The authors thank Drs. Wolfgang Nitschke, William A. Cramer, Antony R. Crofts, and Sergio E. Martinez for important discussions and Dr. William A. Cramer for access to unpublished material. The use of the atomic absorption spectrometer at the WSU Animal Sciences Department is gratefully acknowledged.

REFERENCES

1. Gennis, R. B., Barquera, B., Hacker, B., Van Doren, S. R., Arnaud, S., Crofts, A. R., Davidson, E., Gray, K. A., and Daldal, F. (1993) *J. Bioenerg. Biomembr. 25*, 195−209.

2. Brandt, U., and Trumpower, B. (1994) *Crit. Rev. Biochem. Mol. Biol. 29*, 165−197.
3. Hauska, G., Schütz, M., and Büttner, M. (1996) in *Oxygenic Photosynthesis: The Light Reactions* (Ort, D. R., and Yocum, C. F., Eds.).
4. Liebl, U., Rutherford, W. A., and Nitschke, W. (1990) *FEBS Lett. 261*, 427−430.
5. Nitschke, W., Liebl, U., Matsuura, K., and Kramer, D. M. (1995) *Biochemistry 34*, 11831−11839.
6. Kramer, D. M., Schoepp, B., Liebl, U., and Nitschke, W. (1997) *Biochemistry 36*, 4203−4211.
7. Xiong, J., Inoue, K., and Bauer, C. (1998) *Proc. Natl. Acad. Sci. U.S.A. 95*, 14851−14856.
8. Cramer, W. A., Martinez, S. E., Huang, D., Tae, G.-S., Everly, R. M., Heymann, J. B., Cheng, R. H., Baker, T. S., and Smith, J. L. (1994) *J. Bioener. Biomembr. 26*, 31−47.
9. Martinez, S. E., Huang, D., Szczepaniak, A., Cramer, W. A., and Smith, J. L. (1994) *Structure 2*, 95−105.
10. Carrell, C., Schlarb, B., Bendall, D., Howe, C., Cramer, W. A., and Smith, J. (1999) *Biochemistry 38*, 9590−9599.
11. Mitchell, P. (1975) *FEBS Lett. 59*, 137−139.
12. Mitchell, P. (1975) *FEBS Lett. 56*, 1−6.
13. Crofts, A. R., and Wang, Z. (1989) *Photosynth. Res. 22*, 69−87.
14. Trumpower, B. L. (1990) *J. Biol. Chem. 265*, 11409−11412.
15. Kallas, T. (1994) in *The Molecular Biology of Cyanobacteria* (Bryant, D. A., Ed.) pp 259−317, Kluwer Academic Publishers, Dordrecht, The Netherlands.
16. Brandt, U. (1996) *Biochim. Biophys. Acta 1275*, 41−46.
17. Brandt, U. (1998) *Biochim. Biophys. Acta 1365*, 261−268.
18. Xia, D., Yu, C.-A., Kim, H., Xia, J.-Z., and Kachurin, A. M. (1997) *Science 277*, 60−65.
19. Zhang, Z., Huang, L., Shulmeister, V. M., Chi, Y., Kim, K. K., Hung, L., Crofts, A. R., Berry, E. A., and Kim, S. (1998) *Nature 392*, 677−684.
20. Yu, C., Xia, D., Kim, H., Deisenhofer, J., Zhang, L., Kachurin, A., and Yu, L. (1998) *Biochim. Biophys. Acta 1365*, 151−158.
21. Iwata, S., Lee, J. W., Okada, K., Lee, J. K., Iwata, M., Rasmussen, B., Link, T. A., Ramaswamy, S., and Jap, B. K. (1998) *Science 281*, 64−71.
22. Kim, E., Lowenson, J. D., MacLaren, D. C., and Clarke, S. (1997) *Proc. Natl. Acad. Sci. U.S.A. 94*, 6132−6137.
23. Crofts, A. R., Barquera, B., Gennis, R. B., Kuras, R., Guergova-Kuras, M., and Berry, E. (1997) in *The Phototrophic Prokaryotes* (Peschek, G., Loeffelhardt, W., and Schmetterer, G., Eds.) pp 229−239, Plenum Publ. Corp, New York, London, Washington, DC, Boston.
24. Crofts, A., Berry, E., Kuras, R., Guergova-Kuras, M., Hong, S., and Ugulava, N. (1999) in *Photosynthesis: Mechanisms and Effects* (Garab, G., Ed.) pp 1481−1486, Kluwer Academic Publ., Dordrecht, The Netherlands.
25. Schoepp, B., Brugna, M., Riedel, A., Nitschke, W., and Kramer, D. (1999) *FEBS Lett. 450*, 245−250.
26. Brugna, M., Nitschke, W., Asso, M., Guigliarelli, B., Lemesle-Meunier, D., and Schmidt, C. (1999) *J. Biol. Chem. 274*, 16766−16772.
27. Martinez, S. E., Huang, D., Ponomarev, M., Cramer, W. A., and Smith, J. L. (1996) *Protein Sci. 5*, 1081−1092.
28. Ponamarev, M., and Cramer, W. (1998) *Biochemistry 37*, 17199−17208.
29. Joliot, P., and Joliot, A. (1986) *Photosynth. Res. 9*, 113−124.
30. Joliot, P., and Joliot, A. (1986) *Biochim. Biophys. Acta 849*, 211−222.
31. Joliot, P., and Joliot, A. (1998) *Biochemistry 37*, 10404−10410.
32. Rich, P. R. (1988) *Biochim. Biophys. Acta 932*, 33−42.
33. Kramer, D. M. a. C., A. R. (1990) *Biochim. Biophys. Acta 1183*, 72−84.
34. Yu, S.-G., Romanowska, E., Xue, Z.-t., and Albertsson, P.-Å. (1994) *Biochim. Biophys. Acta 1185*, 239−242.
35. Gu, L.-Q., Yu, L., and Yu, C.-A. (1989) *J. Biol. Chem. 264*, 4506−4512.
36. Bouges-Bocquet, B. (1981) *Biochim. Biophys. Acta 635*, 327−340.
37. van Kooten, O., van Gloudemans, A. G. M., and Vredenberg, W. J. (1983) *Photobiochem. Photobiophys. 6*, 9−14.
38. Moss, D. A., and Bendall, D. S. (1984) *Biochim. Biophys. Acta 767*, 389−395.
39. Ort, D. R. (1986) in *Encyclopedia of Plant Physiology* (Staehelin, L. A., and Arntzen, C. J., Eds.) pp 143−196, Springer, Heidelberg, FRG.
40. Cramer, W. A., Widger, W. R., Black, M. T., and Girvin, M. (1987) in *The Light Reactions* (Barber, J., Ed.) pp 447−493, Elsevier, Amsterdam.
41. Furbacher, P. N., Girvin, M. E., and Cramer, W. A. (1989) *Biochemistry 28*, 8990−8997.
42. Berry, S., and Rumberg, B. (1995) in *Photosynthesis: From Light to Biosphere* (Mathis, P., Ed.) pp 147−150, Kluwer Academic Publishers, Dordrecht, The Netherlands.
43. Berry, S., and Rumberg, B. (1996) *Biochim. Biophys. Acta 1276*, 51−59.
44. Kramer, D. M., Sacksteder, C. A., and Cruz, J. A. (1999) *Photosynth. Res. 60*, 151−163.
45. Kramer, D. M., and Sacksteder, C. A. (1998) *Photosynth. Res. 56*, 103−112.
46. Sacksteder, C. A., Herbert, S., and Kramer, D. M. (1998) in *Photosynthesis: Mechanisms and Effects* (Garab, G., Ed.) pp 1621−1624, Kluwer Academic Publishers, Dordrecht, The Netherlands.
47. von Jagow, G., and Link, T. A. (1986) *Methods Enzymol. 126*, 253−271.
48. Crofts, A. R. (1985) in *The Enzymes of Biological Membranes* (Martonosi, A. N., Ed.) pp 347−382, Plenum Publishing Corp., New York.
49. Izawa, S. (1977) *Encycl. Plant Physiol. 5*, 266−282.
50. Rich, P. R., Madgwick, S. A., Brown, S., von Jagow, G., and Brandt, U. (1992) *Photosynth. Res. 34*, 465−477.
51. Iwata, S., Saynovit, M., Link, T. A., and Michel, H. (1996) *Structure 4*, 567−579.
52. Skulachev, V. P., Christyakov, V. V., Jasaitis, A. A., and Smirnova, E. G. (1967) *Biochem. Biophys. Res. Commun. 26*, 1−6.
53. Link, T. A., and von Jagow, G. (1995) *J. Biol. Chem. 270*, 25001−25006.
54. Rao, B. K. S., Tyryshkin, A. M., Bowman, M. K., and Kramer, D. M. (1998) in *Photosynthesis: Mechanisms and Effects* (Garab, G., Ed.) pp 1569−1572, Kluwer Academic Publishers, Dordrecht, The Netherlands.
55. Kramer, D. M., and Crofts, A. R. (1993) *Biochim. Biophys. Acta 1183*, 72−84.
56. Arnon, D. I. (1949) *Plant Physiol. 24*, 1−15.
57. Hurt, E., and Hauska, G. (1981) *Eur. J. Biochem. 117*, 591−599.
58. Renganathan, M., and Bose, S. (1990) *Photosynth. Res. 23*, 95−99.
59. Metzger, S. U., Cramer, W. A., and Whitmarsh, J. (1997) *Biochim. Biophys. Acta 1319*, 233−241.
60. Kramer, D. M., Joliot, A., Joliot, P., and Crofts, A. R. (1994) *Biochim. Biophys. Acta* 251−262.
61. Redfearn, E. R. (1965) in *Biochemistry of Quinones* (Morton, R. A., Ed.) pp 149−181, Academic Press, London, New York.
62. Atteia, A., de Vitry, C., Pierre, Y., and Popot, J. L. (1992) *J. Biol. Chem. 267*, 226−234.
63. Hofer, P., Grupp, A., Nebenfur, H., and Mehring, M. (1986) *Chem. Phys. Lett. 132*, 279.
64. Shane, J. J., Hofer, P., Reijerse, E. J., and de Boer, E. (1992) *J. Magn. Reson. 99*, 596−604.
65. Gemperle, C., Aebli, G., Schweiger, A., and Ernst, R. R. (1990) *J. Magn. Reson. 88*, 241.
66. Davies, E. R. (1974) *Phys. Lett. 47A*, 1−2.
67. Kevan, L., and Schwarts, R. N. (1979) *Time Domain Electron Spin Resonance*, Wiley, New York.
68. Segel, I. H. (1975) *Enzyme Kinetics*, John Wiley and Sons, New York.
69. Rich, P. (1982) in *Function of Quinones in Energy Conserving Systems* (Trumpower, B. L., Ed.) pp 73−86, Academic Press, New York.
70. Brandt, U. (1996) *FEBS Lett. 387*, 1−6.

71. Ugulava, N. B., and Crofts, A. R. (1998) *FEBS Lett. 440*, 409−413.
72. Crofts, A., Hong, S., Ugulava, N., Barquera, B., Gennis, R., Guergova-Kuras, M., and Berry, E. (1999) *Proc. Natl. Acad. Sci. U.S.A. 96*, 10021−10026.
73. Link, T. A. (1997) *FEBS Lett. 412*, 257−264.
74. Barón, M., Arellano, J. B., and Gorgé, J. L. (1995) *Physiol. Plant. 94*, 174−180.
75. Salerno, J. C., McGill, J. W., and Gerstle, G. C. (1983) *FEBS Lett. 162*, 257−261.
76. Riedel, A., Rutherford, A. W., Hauska, G., Müller, A., and Nitschke, W. (1991) *J. Biol. Chem. 266*, 17838−17844.
77. Nitschke, W., Joliot, P., Liebl, U., Rutherford, A. W., Hauska, G., Müller, A., and Riedel, A. (1992) *Biochim. Biophys. Acta 1102*, 266−268.
78. Mims, W. B. (1968) *Phys. Rev. Lett. 168*, 370.
79. Zhidomirov, G. M., and Salikhov, K. M. (1969) *Zh. Exp. Teor. Fiz. 56*, 1933.
80. Salikov, K. M., Dzuba, S. A., and Raitsimring, A. M. (1981) *J. Magn. Reson. 42*, 255.
81. Schunemann, V., Trautwein, A. X., Illerhaus, J., and Haehnel, W. (1999) *Biochemistry 38*, 8981−8991.
82. Mims, W. B., and Peisach, J. (1981) in *Biological Magnetic Resonance* (Berliner, L. J., and Reuben, J., Eds.) pp 213−263, Plenum, New York.
83. Rowan, L. G., Hahn, E. L., and Mims, W. B. (1965) *Phys. Rev. A 137*, 61.
84. Mims, W. B. (1972) *Phys. Rev. B 5*, 2409−2419.
85. Mims, W. B. (1972) *Phys. Rev. B 5*, 3543−3545.
86. Mims, W. B., and Peisach, J. (1978) *J. Chem. Phys. 69*, 4921−4930.
87. McCraken, J., Pember, S., Benkovic, S. J., Villafranca, J. J., Miller, R. J., and Peisach, J. (1988) *J. Am. Chem. Soc. 110*, 1069.
88. Dikanov, S. A., and Tsvetkov, Y. D. (1992) *Electron Spin Envelope Modulation (ESEEM) Spectroscopy*, CRC, Boca Raton, FL.
89. Flanagan, H. L., Gerfen, G. J., Lai, A., and Singel, A. J. (1988) *J. Chem. Phys. 88*, 2162.
90. Ashby, C. I. H., Cheng, C. P., and Brown, T. L. (1978) *J. Am. Chem. Soc. 100*, 6057−6063.
91. Grupp, A., and Mehring, M. (1990) in *Modern Pulsed and Continuous-Wave Electron Spin Resonance* (Kevan, L., and Bowman, M. K., Eds.) pp 195−230, Wiley, New York.
92. Fan, C., Doan, P. E., Davoust, C. E., Hoffman, B. M. (1992) *J. Magn. Reson. 98*, 62.
93. Cedeno-Maldonado, A., and Swader, J. A. (1972) *Plant Physiol. 50*, 698−701.
94. Samuelsson, G., and Öquist, G. (1980) *Plant Cell Physiol. 21*, 445−454.
95. Shioi, Y., Tamai, H., and Sasa, T. (1978) *Plant Cell Physiol. 19*, 203−29.
96. Hsu, B., and Lee, J. (1988) *Plant Physiol. 87*, 116−119.
97. Vierke, G., and Struckmeier, P. (1978) *Z. Naturforsch 33c*, 266−270.
98. Yruela, I., Alfonso, M., de Zarate, I. O., Montaya, G., and Picorel, R. (1993) *J. Biol. Chem. 268*, 1684−1689.
99. Bohner, H., Bohme, H., and Boger, P. (1980) *Biochim. Biophys. Acta 592*, 103−112.
100. Singh, D., and Singh, S. P. (1987) *Plant Physiol. 83*, 12−14.
101. Utschig, L. M., Ohigashi, Y., Thurnauer, M. C., and Tiede, D. M. (1998) *Biochemistry 37*, 8278−8281.
102. Paddock, M. L., Graige, M. S., Feher, G., and Okamura, M. Y. (1999) *Proc. Natl. Acad. Sci. U.S.A. 96*, 6183−6188.
103. Higgins, D. G., Bleasby, A. J., and Fichs, R. (1991) *CABIOS 8*, 189−191.
104. Holm, L., and Sander, C. (1998) *Nucleic Acids Res 26*, 316−319.
105. Holm, L., and Sander, C. (1996) *Nucleic Acids Res 24*, 207−210.
106. Holm, L., and Sander, C. (1994) *Nucleic Acids Res 22*, 3600−3609.
107. Holm, L., and Sander, C. (1994) *Proteins 19*, 165−173.
108. Cramer, W. A., Martinez, S. E., Huang, D., Tae, G.-S., Everly, R. M., Heymann, J. B., Cheng, R. H., Baker, T. S., and Smith, J. L. (1994) *J. Bioenerg. Biomembr. 26*, 31−47.
109. Crowder, M. S., Prince, R. C., and Bearden, A. (1982) *FEBS Lett. 144*, 204−208.
110. Bergstrom, J., and Vanngard, V. (1982) *Biochim. Biophys. Acta 682*, 452−456.
111. Ubbink, M., Ejdeback, M., Karlsson, B. G., and Bendall, D. S. (1998) *Structure 6*, 323−335.
112. Fernandez-Velasco, J. G., Zhou, J., and Malkin, R. (1997) *Biophys. J. 72A*, 126.
113. Iwata, S., Saynovitis, M., Link, T., and Michel, H. (1996) *Structure 4*, 561−571.
114. Yu, C.-A., Xia, J.-Z., Kachurin, A. M., Yu, L., Xia, D., Kim, H., and Deisenhofer, J. (1996) *Biochim. Biophys. Acta 1275*, 47−53.
115. Mosser, G., Breyton, C., Olofsson, A., Popot, J.-L., and Rigaud, J.-L. (1997) *J. Biol. Chem. 272*, 20263−20268.
116. Soriano, G. M., Ponamarev, M. V., Carrell, C. J., Xia, D., Smith, J. L., and Cramer, W. A. (1999) *J. Bioenerg. Biomembr.* (in press).
117. Malkin, R. (1981) *Isr. J. Chem. 21*, 301−305.
118. Malkin, R. (1986) *FEBS Lett. 208*, 317−320.
119. Chain, R., and Malkin, R. (1979) *Biochemistry 197*, 52−56.
120. Rao, B. K. S. (1999) Ph.D. Thesis, Washington State University, Pullman, WA.

BI991974A